applied sciences

MDPI

Article

Non-Classical Correlations Beyond Entanglement in Noisy Hyperfine Systems: Dynamics of Quantum Dissonance and One-Way Deficit Under Dephasing and Dissipation

Kamal Berrada and Smail Bougouffa *

Department of Physics, College of Science, Imam Mohammad Ibn Saud Islamic University (IMSIU), P.O. Box 90950, Riyadh 11623, Saudi Arabia; kaberrada@imamu.edu.sa
* Correspondence: sbougouffa@imamu.edu.sa

Abstract

We examine non-classical correlations in separable systems through quantum dissonance and one-way quantum deficit. Our study focuses on the generation and dynamics of these correlations in hydrogen atoms influenced by dephasing and dissipative decoherence. We treat the electron–proton spin coupling in the hyperfine structure as a two-qubit quantum system, showing that quantum dissonance and a one-way deficit can emerge from initially classical configurations via this interaction. We further analyze the time evolution of the quantum dissonance and the one-way quantum deficit under dephasing and dissipative quantum dynamics. The results indicate that both measures exhibit a relatively slow decay under decoherence, highlighting their robustness against environmental effects. These insights highlight the promise of hydrogen atoms for robust quantum information protocols in noisy environments.

Keywords: quantum dissonance; one-way quantum deficit; hydrogen atom; hyperfine structure; decoherence; phase damping; dissipative dynamics; non-classical correlations; Lindblad equation

PACS: 03.67.Mn; 03.65.Yz; 42.50.-p; 71.55.Jv

1. Introduction

In quantum theory, the density matrix of a bipartite composite system is classified into four fundamental categories based on the type of correlations between its subsystems: product states, classical states, separable states, and entangled states [1]. Classical correlations appear in every category except pure product states, where no correlations between subsystems exist. By contrast, quantum correlations are not confined to entangled states alone; they can also appear in specific separable states, namely those convex mixtures of product states whose joint statistics cannot be reproduced solely through classical probability distributions. A fundamental challenge in quantum foundations lies in sharply distinguishing genuine quantum correlations from merely classical ones. For many years, research predominantly emphasized the boundary between entanglement and separability, since entanglement was long considered the primary resource enabling quantum information tasks and quantum computation [2]. Entanglement serves as a vital ingredient for numerous quantum protocols, such as quantum teleportation [3], superdense coding [4], quantum key distribution [5], and remote state preparation [6,7]. More recently, however, it has been recognized that valuable quantum correlations can persist even in the absence of

Check for updates

Received: 1 April 2026
Revised: 14 May 2026
Accepted: 18 May 2026
Published: 22 May 2026

Copyright: © 2026 by the authors. Licensee MDPI, Basel, Switzerland. This article is an open access article distributed under the terms and conditions of the Creative Commons Attribution (CC BY) license.

entanglement. This insight was formalized through the introduction of quantum discord by Henderson and Vedral [8] and Ollivier and Zurek [9]. Subsequent works have further explored and generalized different forms of non-classical correlations and their operational significance [10–12], including analytical studies for specific classes of states [13].

Among the leading indicators of such non-classical correlations is quantum discord, which quantifies the discrepancy between the total quantum mutual information and the largest classical mutual information achievable via optimal local projective measurement on one subsystem. For two-qubit systems, obtaining an analytical expression for discord remains highly nontrivial in general [13–17]. In addition to entanglement and discord, various alternative figures of merit for quantum correlations have emerged, including quantum deficit [18,19], measurement-induced disturbance [20], geometric discord [21,22], and discord for continuous-variable systems [23,24]. Modi et al. [1] proposed a unified geometric approach, defining each correlation type as the minimal relative entropy distance from the given state to the closest state lacking that specific property. Because all distances rely on relative entropy, this framework allows consistent comparisons across different correlation measures. The distance is computed to the nearest state that does not possess the property under consideration. In this setting, a novel quantity termed quantum dissonance was introduced to characterize quantum correlations remaining in states after entanglement has been eliminated. Strictly, in entangled regimes, dissonance does not always coincide with discord minus entanglement, as the two may rely on distinct optimization procedures. Nonetheless, dissonance and discord share qualitative features, both capturing quantum correlations beyond classical descriptions in separable regimes. For any separable state (where entanglement vanishes), quantum dissonance precisely equals quantum discord.

The hydrogen atom features a very basic structure and has been a key foundation for grasping quantum mechanics since its beginnings. It offers a deep understanding of how electrons and nuclei behave in areas such as physics, chemistry, and biology [25–28].

Beyond its foundational importance in the theory of quantum physics, this atom offers significant potential for applications in quantum information science, considered as an accessible model system for investigating non-classical correlations. The spins of the proton and the electron in a hydrogen atom create a simple system with two quantum bits (qubits). This setup has a clear mathematical space (Hilbert space) that makes it easy to examine the quantum correlations between them. When the temperature is low enough, the energy levels linked to the hyperfine interaction in hydrogen show natural quantum entanglement. As temperature increases, this entanglement drops quickly and vanishes entirely once the thermal energy surpasses a specific value, roughly $\tau_c \approx 5.35\,\mu\text{eV}$. This critical point comes from the way the system reaches thermal balance across the hyperfine energy states, where the amount of quantum entanglement depends on the balance between the thermal energy available and the size of the hyperfine energy difference [29–31].

Contemporary investigations have revealed distinct phases featuring pronounced nuclear spin polarization in hydrogen atoms confined within solid molecular hydrogen matrices [29,32]. These phases deviate significantly from the classical Boltzmann distribution of level populations at ultra-low temperatures [29–31], thereby stimulating key questions regarding the role of quantum effects in such confined atomic environments. The proton–electron spin pair in hydrogen constitutes a valuable platform for probing non-classical correlations and their relevance to quantum information processing tasks. Analogous systems, such as electron spins in double quantum dots containing two electrons, have demonstrated qubit functionality in quantum technologies [33–37]. Likewise, nuclear spins—particularly those associated with nitrogen-vacancy centers in diamond—have established themselves as powerful resources in the framework of quantum information processing [38–41].

Open quantum systems theory investigates how quantum entities evolve when coupled to external reservoirs, a topic central to quantum mechanics since its early formulations [42]. Although substantial advancements have been made in theoretical modeling, core difficulties persist, particularly with decoherence—the irreversible erosion of quantum superposition due to exchanges with the surroundings. This mechanism has drawn intense scrutiny in quantum information science and computing, as it constitutes a primary obstacle to implementing scalable quantum processors [2,43,44]. The temporal behavior of quantum correlations under such influences has become a major research focus in applied contexts. The principal objective of the present work is to examine the emergence and subsequent time development of non-classical correlations—namely quantum dissonance and one-way quantum deficit—within the electron–proton hyperfine spin configuration of hydrogen atoms subjected to Markovian phase-damping and amplitude-damping channels. By modeling the intrinsic spin-spin interaction as an effective two-qubit dynamics, we establish through exact analytical derivations and numerical simulations that these authentic quantum features can arise naturally from starting separable states with only classical correlations, displaying substantially enhanced stability relative to standard entanglement quantifiers when exposed to pure dephasing or relaxation noise. Through explicit time-dependent solutions for the density matrix in its characteristic X-form structure, together with precise evaluations of relative-entropy-based measures, we uncover unique evolutionary patterns, including temporary amplification of dissonance in regimes of mild phase damping and extended persistence of one-way deficit even amid intense environmental perturbations. These observations illuminate the ordering of decay rates among various quantum correlation types in noisy bipartite spin environments, while emphasizing the hydrogen atom's intrinsic suitability as a robust, naturally occurring candidate for quantum information tasks resilient to realistic noise sources.

The present manuscript is structured as follows: Section 2 presents the physical model of the hydrogen atom, detailing the magnetic spin-spin Hamiltonian for the electron–proton hyperfine interaction and its exact diagonalization. Section 3 treats pure phase decoherence via local Lindblad dephasing channels and derives closed-form time evolution for X-structured states. Section 4 extends the analysis to dissipative decoherence using spin-flip Lindblad operators, again obtaining exact analytical solutions. Section 5 defines the quantum dissonance and one-way quantum information deficit within the relative-entropy framework and provides their exact expressions for both noise models. Section 6 presents numerical results demonstrating the emergence, transient enhancement under dephasing, and superior robustness of these non-classical correlations compared to entanglement. Finally, Section 7 concludes with the main findings and their implications for decoherence-resilient quantum information processing in atomic hydrogen.

2. Spin–Spin Hamiltonian and Quantum States in Hydrogen Atom

Hydrogen Atomic Fine Structure

In the hydrogen atom, the hyperfine structure arises from the magnetic interaction between the tiny magnetic moments produced by the electron's spin and the proton's spin. When the atom is in its lowest energy state (the 1s orbital), the electron has no orbital angular momentum in the sense that $\langle \mathbf{L} \rangle = 0$, and there is no classical orbital current around the nucleus. Consequently, there is no contribution to the magnetic field at the nucleus arising from orbital motion. As a result, the dominant contribution to the hyperfine splitting originates from the direct magnetic interaction between the intrinsic spin magnetic moments of the proton and the electron [28].

This spin–spin interaction provides the famous 21 cm emission line, corresponding to 1420 MHz in transition frequency, which is of fundamental significance in atomic

spectroscopy and radio astronomy [45]. This interaction is well described employing first-order perturbation theory. It involves a small correction term in the Hamiltonian that depends on the dot product of the nuclear spin operator and the electronic spin operator:

$$\mathcal{H}_{\mathrm{m}} \propto \vec{\mu}_N \cdot \vec{\mu}_e,$$

where the operators $\vec{\mu}_N$ and $\vec{\mu}_e$ stand, respectively, for the nuclear spin (proton) and the electron spin. In the existence of an external magnetic field, the hyperfine Hamiltonian is extended by considering the Zeeman term [45–47].

For a proton and an electron, the effective magnetic (hyperfine) Hamiltonian can be expressed using Pauli matrices as

$$\begin{aligned} \mathcal{H}_{\mathrm{M}} &= \alpha\, \vec{\tau}_N \cdot \vec{\tau}_e \\ &= \alpha\big(\tau_x^{(N)}\tau_x^{(e)} + \tau_y^{(N)}\tau_y^{(e)} + \tau_z^{(N)}\tau_z^{(e)}\big), \end{aligned} \tag{1}$$

where the parameter α represents the coupling constant, while $\vec{\tau}_N = (\tau_x^{(N)}, \tau_y^{(N)}, \tau_z^{(N)})$ and $\vec{\tau}_e = (\tau_x^{(e)}, \tau_y^{(e)}, \tau_z^{(e)})$ operate, respectively, on the spin spaces of nuclear and electron.

The hyperfine coupling constant in the hydrogen atom is expressed explicitly as [45]:

$$\alpha = \frac{\mu_0\, g_e\, g_p\, e^2\, \hbar^2}{12\pi\, m_e\, m_p\, a_0^3},$$

where μ_0 stands for the permeability of the free space, a_0 denotes the Bohr radius, g_p (m_p) and g_e (m_e) are the g-factors (masses) of the electron and proton, respectively. This expression quantifies the magnitude of the magnetic dipole–dipole coupling (also called the hyperfine interaction) that occurs between the spin of the electron and the spin of the proton. Its value depends directly on how large the electron's probability density is right at the location of the nucleus.

Each spin-1/2 particle possesses a 2-dimensional Hilbert space. For the electron this space is spanned by the states $|\uparrow_e\rangle$ and $|\downarrow_e\rangle$, while for the nucleus it is spanned by $|\uparrow_N\rangle$ and $|\downarrow_N\rangle$. The Hilbert space of the coupled electron–nucleus system is therefore the tensor product

$$\mathcal{S} = \mathcal{S}_e \otimes \mathcal{S}_N,$$

which is four-dimensional and has the product basis

$$|\uparrow_e\uparrow_N\rangle\,, \quad |\uparrow_e\downarrow_N\rangle\,, \quad |\downarrow_e\uparrow_N\rangle\,, \quad |\downarrow_e\downarrow_N\rangle\,.$$

Diagonalization of the magnetic hyperfine Hamiltonian $\mathcal{H}_{\mathrm{M}}$ yields one antisymmetric singlet eigenstate

$$|\Psi_-\rangle = \frac{1}{\sqrt{2}}\Big(|\uparrow_e\downarrow_N\rangle - |\downarrow_e\uparrow_N\rangle\Big) \tag{2}$$

with energy $E_- = -3\alpha$, together with a degenerate symmetric triplet manifold consisting of the three states

$$|\Phi_+\rangle = |\uparrow_e\uparrow_N\rangle\,, \qquad E_+ = +\alpha, \tag{3a}$$

$$|\Phi_0\rangle = \frac{1}{\sqrt{2}}\Big(|\uparrow_e\downarrow_N\rangle + |\downarrow_e\uparrow_N\rangle\Big), \qquad E_0 = +\alpha, \tag{3b}$$

$$|\Phi_-\rangle = |\downarrow_e\downarrow_N\rangle\,, \qquad E_- = +\alpha. \tag{3c}$$

The energy separation between the singlet and the triplet manifold is therefore

$$\Delta E = E_{\Phi} - E_{-} = 4\alpha,$$

where $E_{\Phi} = \alpha$ denotes the common energy of the triplet states.

Although the hyperfine interaction in a single hydrogen atom is intrinsically weak compared to other atomic energy scales, the present model should be understood as an effective two-qubit spin description capturing the essential structure of electron–nucleus spin correlations. Such effective spin–spin Hamiltonians are not limited to atomic hydrogen, but are widely realized in a variety of controllable quantum platforms, including trapped ions, nuclear magnetic resonance systems, and solid-state spin devices, where hyperfine-like couplings and decoherence processes can be engineered and tuned experimentally. In this context, the model provides a general framework for studying the dynamics of quantum correlations under the combined action of coherent spin interactions and environmental noise, rather than a prediction of specific spectroscopic effects in isolated hydrogen atoms.

3. Phase Decoherence in Hydrogen Hyperfine Qubits

Phase decoherence constitutes a core environmental noise mechanism in quantum mechanics, whereby interactions with the surroundings erase relative phase information among coherent superpositions while leaving the diagonal populations of the density matrix unchanged during the evolution. According to the hydrogen atom's hyperfine magnetic coupling, such noise arises intrinsically from differential couplings of the proton and electron spin components to fluctuating external magnetic fields or other perturbations. To provide a quantitative description of these processes, the present study adopts the Lindblad master equation (LME) formalism, incorporating local collapse operators of the τ_z Pauli type. These operators are designed to damp off-diagonal coherences selectively, without inducing transitions that would modify the occupation probabilities of energy eigenstates.

3.1. Lindblad Equation for Phase Damping

The density matrix $\varrho(t)$ changes in time according to the LME [48–50]:

$$\frac{d\varrho}{dt} = -i[\mathcal{H}_{\mathrm{M}}, \varrho] + \mathcal{L}(\varrho), \tag{4}$$

where the term $\mathcal{H}_{\mathrm{M}}$ denotes the Hamiltonian associated with magnetic interactions, and $\mathcal{L}(\varrho)$ is the dissipative superoperator responsible for environmental effects.

For pure phase damping, we define the local Lindblad operators:

$$M_e = \tau_z^e \otimes \mathbb{I}_N, \qquad M_N = \mathbb{I}_e \otimes \tau_z^N, \tag{5}$$

with associated damping coefficients κ_e and κ_N. The dissipator then becomes

$$\mathcal{L}(\varrho) = \kappa_e(M_e \varrho M_e - \varrho) + \kappa_N(M_N \varrho M_N - \varrho), \tag{6}$$

which simplifies due to the property $M_e^2 = M_N^2 = \mathbb{I}$, characteristic of Pauli operators.

3.2. Dynamic Equations for Density Matrix Components

Let us define the parameter $\Omega = \alpha/\hbar$, which represents the coupling strength of the coherent interaction between the nuclear spin and the electron spin.

Under the influence of pure phase-damping noise, the time development of the matrix elements $\varrho_{mn}(t)$ is governed by a set of differential equations.

Population Dynamics:

$$\frac{d\varrho_{11}}{dt} = 0, \tag{7}$$
$$\frac{d\varrho_{22}}{dt} = -2i\Omega(\varrho_{23} - \varrho_{32}), \tag{8}$$
$$\frac{d\varrho_{33}}{dt} = 2i\Omega(\varrho_{23} - \varrho_{32}), \tag{9}$$
$$\frac{d\varrho_{44}}{dt} = 0. \tag{10}$$

Coherence Evolution:

$$\frac{d\varrho_{12}}{dt} = -2i\Omega(\varrho_{12} - \varrho_{13}) - 2\kappa_N\varrho_{12}, \tag{11}$$
$$\frac{d\varrho_{13}}{dt} = -2i\Omega(\varrho_{13} - \varrho_{12}) - 2\kappa_e\varrho_{13}, \tag{12}$$
$$\frac{d\varrho_{14}}{dt} = -2(\kappa_e + \kappa_N)\varrho_{14}, \tag{13}$$
$$\frac{d\varrho_{23}}{dt} = -2i\Omega(\varrho_{22} - \varrho_{33} + \varrho_{23}) - 2(\kappa_e + \kappa_N)\varrho_{23}, \tag{14}$$
$$\frac{d\varrho_{24}}{dt} = -2i\Omega(\varrho_{24} - \varrho_{34}) - 2\kappa_e\varrho_{24}, \tag{15}$$
$$\frac{d\varrho_{34}}{dt} = -2i\Omega(\varrho_{24} - \varrho_{34}) - 2\kappa_N\varrho_{34}, \tag{16}$$

with $\varrho^*_{mn} = \varrho_{nm}$. These equations clearly show the main features of pure phase damping: the populations remain constant, while the off-diagonal coherence terms decay exponentially with time. In particular, the coupling among ϱ_{22}, ϱ_{33}, and ϱ_{23} demonstrates how the gradual loss of coherence leads to direct population transfer between different entangled states.

In the following step, we study the time development of non-classical correlations through a numerical solution of these equations with physically relevant initial states.

3.3. Initial Quantum State and Dynamics

We study the time development of correlations in the proton–electron system when it interacts with a Markovian environment. For this purpose, we focus on a particular group of two-qubit states, known as X-states. These states can be realistically created in physical setups and are straightforward to generate and detect in laboratory experiments. Because of these features, they serve as valuable resources for various quantum information applications, including quantum teleportation, and secure key sharing through quantum cryptography [4,51,52].

A general X-state can be written in the following form, using three real parameters b_1, b_2, b_3 that each lie in the interval $[-1, 1]$:

$$\varrho(0) = \frac{1}{4}\begin{pmatrix} 1+b_3 & 0 & 0 & b_1-b_2 \\ 0 & 1-b_3 & b_1+b_2 & 0 \\ 0 & b_1+b_2 & 1-b_3 & 0 \\ b_1-b_2 & 0 & 0 & 1+b_3 \end{pmatrix}. \tag{17}$$

This state has the special property that the reduced density matrix for the electron (and also for the nucleus) is completely mixed, i.e., $\varrho_e = \varrho_N = \mathbb{I}/2$. The parametrization covers both the fully entangled Bell states (where $|b_1| = |b_2| = |b_3| = 1$) and Werner states (where

$|b_1| = |b_2| = |b_3| = b$) as particular instances. It therefore allows a thorough investigation of how correlations evolve.

Under the Markovian approximation, which is described by the LME, the time-evolving density matrix $\varrho(t)$ keeps its X-state form throughout the dynamics

$$\varrho(t) = \begin{pmatrix} \varrho_{11}(t) & 0 & 0 & \varrho_{14}(t) \\ 0 & \varrho_{22}(t) & \varrho_{23}(t) & 0 \\ 0 & \varrho_{32}(t) & \varrho_{33}(t) & 0 \\ \varrho_{41}(t) & 0 & 0 & \varrho_{44}(t) \end{pmatrix}, \tag{18}$$

as confirmed by Equations (7) and (11). Keeping the X-state structure during evolution is especially helpful for analytical calculations. This is particularly useful when studying spin-selective decoherence processes, which are common in atomic systems.

To make our work fully clear and complete, we present exact analytical eformulas for the time evolution of the density matrix elements. These solutions are given for several important and physically realistic initial states. Non-vanishing elements are expressed as follows:

$$\varrho_{11}(t) = \varrho_{44}(t) = \tfrac{1}{4}(1 + b_3), \tag{19}$$

$$\varrho_{22}(t) = \varrho_{33}(t) = \tfrac{1}{4}(1 - b_3), \tag{20}$$

$$\varrho_{14}(t) = \tfrac{1}{4}(b_1 - b_2)e^{-2\kappa t}, \tag{21}$$

$$\varrho_{23}(t) = \tfrac{1}{4}(b_1 + b_2)e^{-2\kappa t}. \tag{22}$$

Vanishing elements are expressed as follows:

$$\varrho_{12}(t) = \varrho_{13}(t) = \varrho_{24}(t) = \varrho_{31}(t) = \varrho_{34}(t) = 0, \tag{23}$$

with $\varrho_{mn} = \varrho^*_{nm}$, where $\kappa = \kappa_e + \kappa_N$. Now that we have described how the system evolves under phase damping, we next look at the correlations.

4. Dissipative Processes in Hydrogen Hyperfine Structure

In this section, we analyze the temporal development of the electron–proton spin configuration within the hydrogen atom's hyperfine manifold by adopting the LME approach, which generalizes the coherent Schrödinger dynamics to open-system regimes [53]. This formalism incorporates dissipative terms that effectively describe environmental phase relaxation under Markovian conditions, thereby supplying a robust theoretical scaffold for assessing how quantum correlations withstand noise in evolving quantum environments. The Lindblad structure proves especially advantageous when examining the temporal fate of entanglement within hydrogen's hyperfine levels, as it systematically incorporates mechanisms that perturb unitary evolution and thus permits quantitative evaluation of correlations against realistic environmental perturbations. Moreover, this methodology constitutes a versatile platform for tracking the survival and eventual erosion of correlations encoded in the internal spin degrees of freedom of the hydrogen atom. By explicitly accounting for departures from pure unitary propagation—often explored via related phenomenological extensions like the Milburn model—the Lindblad framework enables detailed exploration of how quantum-to-classical transitions manifest in noisy atomic systems. To apply this description to the hyperfine dynamics, we track the dynamics of $\rho(t)$ in the presence of decoherence processes. The governing evolution equation of the Lindblad type [48–50] is provided in Equation (4).

The Lindblad operators M_k describe the different ways the environment interacts with the system. The first part of the master equation gives the coherent (unitary) time evolution caused by the hyperfine coupling. The second part describes decoherence processes. It assumes a Markovian environment, meaning that the environment has no memory—past interactions do not influence future ones.

The dissipator then becomes

$$\mathcal{L}(\varrho) = \frac{\kappa}{2}\sum_k \left(M_k \varrho(t) M_k^\dagger - \frac{1}{2}\{M_k^\dagger M_k, \rho(t)\} \right), \tag{24}$$

which simplifies due to the property $M_e^2 = M_N^2 = \mathbb{I}$, characteristic of Pauli operators.

In the hyperfine system, decoherence arises mainly from spin-flip events that influence both the electron spin and the proton spin. These processes are described using Lindblad operators, which are defined as follows:

$$\begin{aligned} M_1 &= \tau_+^e \otimes I_N, \quad \text{(electron excitation, } |-_e\rangle \to |+_e\rangle\text{)}, \\ M_2 &= \tau_-^e \otimes I_N, \quad \text{(electron relaxation, } |+_e\rangle \to |-_e\rangle\text{)}, \\ M_3 &= I_e \otimes \tau_+^N, \quad \text{(proton excitation, } |-_p\rangle \to |+_p\rangle\text{)}, \\ M_4 &= I_e \otimes \tau_-^N, \quad \text{(proton relaxation, } |+_p\rangle \to |-_p\rangle\text{)}, \end{aligned} \tag{25}$$

where the Pauli ladder operators are introduced by

$$\tau_+ = \begin{bmatrix} 0 & 1 \\ 0 & 0 \end{bmatrix}, \quad \tau_- = \begin{bmatrix} 0 & 0 \\ 1 & 0 \end{bmatrix}, \tag{26}$$

and I_N, I_e are identity operators. These operators describe spin-flip transitions that can occur between the different spin states.

In the present model, the Lindblad operators M_k describe spin-flip events that act on the electron spin and the proton spin in the hydrogen atom. These spin flips can be caused by different physical mechanisms, such as thermal noise from the surrounding electromagnetic field, random or varying stray magnetic fields, and spontaneous emission due to coupling with vacuum fluctuations

Although we do not describe any particular physical environment in detail, this phenomenological model still includes the main decoherence effects that influence spin behavior under the Markovian approximation. In this work, we mainly consider spin-flip processes—which include both relaxation and excitation—as the dominant source of quantum decoherence. These spin-flip events change the populations of the different spin states and therefore strongly affect measures such as quantum dissonance and one-way quantum deficit.

By writing the LME (4) in the basis $\mathcal{S}$, we arrive at a set of differential equations for the elements $\rho_{ij}(t)$. The equations associated with the diagonal elements are

$$\begin{aligned} \frac{d}{dt}\varrho_{11}(t) &= \kappa(\varrho_{33}(t) + \varrho_{22}(t) - 2\varrho_{11}(t)), \\ \frac{d}{dt}\varrho_{22}(t) &= -i2\Omega(\rho_{32}(t) - \varrho_{23}(t)) + \kappa(\varrho_{44}(t) + \varrho_{11}(t) - 2\varrho_{22}(t)), \\ \frac{d}{dt}\varrho_{33}(t) &= -i2\Omega(\varrho_{23}(t) - \varrho_{32}(t)) + \kappa(\varrho_{44}(t) + \varrho_{11}(t) - 2\varrho_{33}(t)), \\ \frac{d}{dt}\varrho_{44}(t) &= \kappa(\varrho_{22}(t) + \varrho_{33}(t) - 2\varrho_{44}(t)), \end{aligned} \tag{27}$$

where $\Omega = \alpha/\hbar$. For the off-diagonal elements, we have

$$\begin{aligned}
\frac{d}{dt}\varrho_{12}(t) &= -i2\Omega(\rho_{12}(t) - \varrho_{13}(t)) + \gamma(\varrho_{34}(t) - 2\varrho_{12}(t)),\\
\frac{d}{dt}\varrho_{13}(t) &= -i2\Omega(\varrho_{13}(t) - \varrho_{12}(t)) + \gamma(\varrho_{24}(t) - 2\varrho_{13}(t)),\\
\frac{d}{dt}\varrho_{14}(t) &= -2\gamma\varrho_{14}(t),\\
\frac{d}{dt}\varrho_{23}(t) &= -i2\Omega(\rho_{33}(t) - \rho_{22}(t)) - 2\gamma\varrho_{23}(t),\\
\frac{d}{dt}\varrho_{24}(t) &= -i2\Omega(\varrho_{34}(t) - \varrho_{24}(t)) + \gamma(\varrho_{13}(t) - 2\varrho_{24}(t)),\\
\frac{d}{dt}\varrho_{34}(t) &= -i2\Omega(\varrho_{24}(t) - \varrho_{34}(t)) + \gamma(\varrho_{12}(t) - 2\varrho_{34}(t)),
\end{aligned} \tag{28}$$

along with their complex conjugates. These equations show how the populations of the different spin states change and transfer between one another, and how the coherences (off-diagonal elements) decrease over time because of coupling to the environment.

Starting from a coherent superposition state such as (17), the analytical solutions for this initial state yield

$$\begin{aligned}
\varrho_{11}(t) = \varrho_{44}(t) &= \frac{1}{4} + \frac{b_3 e^{-4\kappa t}}{4},\\
\varrho_{22}(t) = \varrho_{33}(t) &= \frac{1}{4} - \frac{b_3 e^{-4\kappa t}}{4},\\
\varrho_{14}(t) &= \frac{(b_1 - b_2)e^{-2\kappa t}}{4},\\
\varrho_{23}(t) &= \frac{(b_1 + b_2)e^{-2\kappa t}}{4},\\
\varrho_{ij}(t) &= 0 \quad \text{for all other } i, j,
\end{aligned} \tag{29}$$

with $\varrho_{mn} = \varrho^*_{nm}$.

With the analytical solutions for the time-dependent density matrix established, we can now systematically characterize the emergence and dynamics of correlations within the hydrogen atom's hyperfine system. These explicit solutions enable us to compute fundamental measures of quantumness, particularly quantum dissonance, which captures non-classical correlations beyond entanglement. In subsequent analysis, we employ these analytical results to examine how quantum dissonance evolves in the electron–proton spin system under both dephasing and dissipative processes within the hyperfine interaction framework.

5. Quantum Dissonance and One-Way Quantum Information Deficit

Having derived in Sections 3 and 4 the exact time-dependent density operator of the electron–proton hyperfine system under both dephasing and dissipative dynamics—solutions that preserve the X-form for arbitrary initial states—we now quantify the genuinely non-classical correlations that persist long after entanglement has decayed to zero. Within the relative-entropy framework of Modi et al. [1], quantum dissonance $D(\rho)$ is defined as the minimal relative entropy to the closest classical-quantum state, exactly coinciding with quantum discord for separable states. The one-way quantum information deficit $\Delta^{\rightarrow}(\rho)$ is introduced as the minimal entropy increase under optimal local measurement on one subsystem. The retained X-structure enables fully analytical expressions for both measures under the two decoherence models. These exact results demonstrate the spontaneous emergence of dissonance and one-way deficit from initially classical states, their transient enhancement under moderate dephasing, and their significantly greater

robustness compared with entanglement, confirming the hydrogen hyperfine system as a naturally resilient carrier of non-classical correlations in noisy environments.

The time evolution of the total system can be written in the Bell basis as

$$\hat{\rho}(t) = \sum_{i=1}^{4} \lambda_i(t) \, |\mathcal{B}_i\rangle\langle\mathcal{B}_i|, \tag{30}$$

where $|\mathcal{B}_i\rangle \in \{|\Psi^+\rangle, |\Phi^+\rangle, |\Phi^-\rangle, |\Psi^-\rangle\}$ denote the Bell states, with $|\Psi^\pm\rangle = (|00\rangle \pm |11\rangle)/\sqrt{2}$ and $|\Phi^\pm\rangle = (|01\rangle \pm |10\rangle)/\sqrt{2}$.

(i) Dephasing (phase damping) case

The eigenvalues evolve as

$$\begin{aligned}
\lambda_1(t) &= \frac{1}{4}\Big[1 + b_3 + (b_1 - b_2)e^{-2\kappa t}\Big], \\
\lambda_2(t) &= \frac{1}{4}\Big[1 - b_3 + (b_1 + b_2)e^{-2\kappa t}\Big], \\
\lambda_3(t) &= \frac{1}{4}\Big[1 - b_3 - (b_1 + b_2)e^{-2\kappa t}\Big], \\
\lambda_4(t) &= \frac{1}{4}\Big[1 + b_3 - (b_1 - b_2)e^{-2\kappa t}\Big].
\end{aligned} \tag{31}$$

This dynamics reflects pure loss of phase coherence, where only the off-diagonal elements of the density matrix decay, while populations remain unchanged.

(ii) Dissipative (amplitude damping) case

The eigenvalues evolve as

$$\begin{aligned}
\lambda_1(t) &= \frac{1}{4}\Big[1 + b_3 e^{-4\kappa t} + (b_1 - b_2)e^{-2\kappa t}\Big], \\
\lambda_2(t) &= \frac{1}{4}\Big[1 - b_3 e^{-4\kappa t} + (b_1 + b_2)e^{-2\kappa t}\Big], \\
\lambda_3(t) &= \frac{1}{4}\Big[1 - b_3 e^{-4\kappa t} - (b_1 + b_2)e^{-2\kappa t}\Big], \\
\lambda_4(t) &= \frac{1}{4}\Big[1 + b_3 e^{-4\kappa t} - (b_1 - b_2)e^{-2\kappa t}\Big].
\end{aligned} \tag{32}$$

In this case, decoherence is accompanied by energy relaxation, leading to simultaneous decay of coherences and populations, which accelerates the loss of quantum correlations compared to pure dephasing.

Since all quantum correlation measures considered in this work, including quantum dissonance and the one-way quantum deficit, are fully determined by the spectrum of the density matrix, the above eigenvalue dynamics directly govern their temporal behavior under both dephasing and dissipative processes.

To quantify quantum correlations, we employ the relative quantum entropy as a measure of distinguishability between two density operators $\hat{\rho}$ and $\hat{\sigma}$. This quantity captures how distinguishable the two quantum states are and is defined as follows:

$$S(\hat{\rho}||\hat{\sigma}) = \mathrm{Tr}(\hat{\rho}\log_2\hat{\rho} - \hat{\rho}\log_2\hat{\sigma}). \tag{33}$$

The classical state closest to the state during the time t is

$$\hat{\rho}_{\mathrm{cl}}(t) = \frac{q(t)}{2}\sum_{i=1,2}|\Psi_i\rangle\langle\Psi_i| + \frac{1-q(t)}{2}\sum_{i=3,4}|\Psi_i\rangle\langle\Psi_i| \tag{34}$$

with $q(t) = \lambda_1(t) + \lambda_2(t)$ such that $\lambda_1(t)$ and $\lambda_2(t)$ are the two largest eigenvalues of the density matrix, and $|\Psi_i\rangle$ are the corresponding Bell states. The term "classical state" is used here in the sense of quantum information theory, referring to states with only classical correlations and have zero quantum discord. Such states are classical mixtures of locally distinguishable states in a given basis. Although Equation (34) is expressed in the Bell basis, it may still represent a classical state, since classicality is determined by the absence of non-classical correlations rather than by the specific decomposition used. In Figures 1 and 2, we show how eigenvalues $\lambda_i(t)$ evolve over time. These eigenvalues represent the populations (probabilities) of each of the four Bell-state components in the evolving quantum state. Quantum dissonance is introduced as the distance between the closest separable state $\hat{\sigma}$ and its closest classical state $\hat{\rho}_{cl}$ [1]. For the state (31), the separable closet state is given by

$$\hat{\sigma} = \sum_{i=1}^{4} p_i |\Psi_i\rangle\langle\Psi_i|. \tag{35}$$

We set $p_1 = 1/2$, while the remaining probabilities are given by $p_i = \lambda_i/[2(1-\lambda_1)]$ for $i = 2, 3, 4$. It can be shown (see Appendix A) that this Bell-diagonal state satisfies the PPT criterion and is therefore separable.

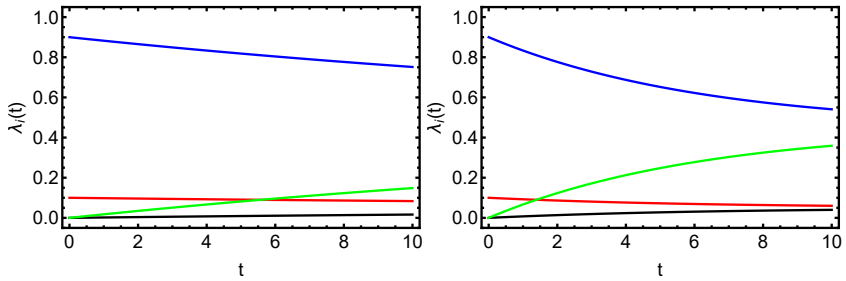


Figure 1. Time evolution of the eigenvalues λ_1 (blue), λ_2 (red), λ_3 (black), and λ_4 (green) of the electron–proton density matrix in the Bell basis for the dephasing case. Panels (**a**,**b**) correspond to the initial conditions $b_1 = 1$, $b_2 = -0.8$, $b_3 = 0.8$ with dephasing rates $\kappa = 0.02\alpha$ and $\kappa = 0.08\alpha$, respectively. Time is measured in units of $1/\alpha$. In this case, decoherence induces a purely coherent decay of off-diagonal contributions, leading to a redistribution of spectral weights without energy relaxation.

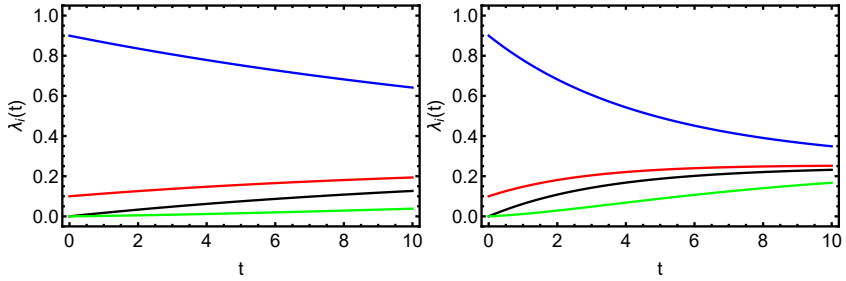


Figure 2. Time evolution of the eigenvalues λ_1 (blue, solid), λ_2 (red), λ_3 (black), and λ_4 (green) of the electron–proton density matrix in the Bell basis for the dissipative case. Panels (**a**,**b**) correspond to the initial conditions $b_1 = 1$, $b_2 = -0.8$, $b_3 = 0.8$ with dissipative rates $\kappa = 0.02\alpha$ and $\kappa = 0.08\alpha$, respectively. Time is measured in units of $1/\alpha$. In contrast to the dephasing case, both coherence loss and population relaxation contribute to the dynamics, resulting in a faster decay and irreversible redistribution of spectral weights toward a mixed steady state.

The quantum dissonance can be computed exactly within the present model through

$$D = 1 + \sum_{i=1}^{4} p_i \log_2 p_i - (p_1 + p_2)\log_2(p_1 + p_2) - (1 - p_1 - p_2)\log_2(1 - p_1 - p_2), \quad (36)$$

where we have used the fact that $D = S(\hat{\rho}_{\mathrm{cl}}) - S(\hat{\sigma})$, with $S(\hat{\rho}_{\mathrm{cl}}) = 1 - q\log_2 q - (1 - q)\log_2(1 - q)$ and $S(\hat{\sigma}) = -\sum_{i=1}^{4} p_i \log_2 p_i$, evaluated in the common Bell basis, with $q = p_1 + p_2$.

To clarify the derivation of Equation (36), we note that the density matrix remains diagonal in the Bell basis during the evolution, such that its spectral decomposition directly provides the eigenvalues $\lambda_i(t)$ associated with the Bell states $|\Psi_i\rangle$. The closest separable state $\hat{\sigma}$ in Equation (35) is therefore also diagonal in the same basis, with probabilities p_i determined by minimizing the relative entropy with respect to the set of separable states.

For Bell-diagonal states, this minimization is achieved by fixing the largest probability to $p_1 = 1/2$, while the remaining probabilities are obtained by a proper normalization of the other eigenvalues, namely $p_i = \lambda_i/[2(1 - \lambda_1)]$ for $i = 2, 3, 4$. This choice ensures that $\hat{\sigma}$ lies on the boundary of the separable set and minimizes the relative entropy distance [1].

Substituting Equation (35) into the definition of the relative entropy and using the Bell-diagonal structure of both $\hat{\sigma}$ and $\hat{\rho}_{\mathrm{cl}}$, the trace can be evaluated straightforwardly in the common eigenbasis. This leads to a closed-form expression in terms of the probabilities p_i, yielding Equation (36).

The concept of quantum deficit arose from a fundamental thermodynamic question: how much additional work can be extracted from a quantum-correlated system in contact with a heat bath when arbitrary global (nonlocal) operations are allowed, compared to the case where only LOCC are permitted [18]. This quantity is closely related to several other measures of quantum correlations. Oppenheim et al. formally introduced the concept of the work (quantum) deficit, defining it as the difference between the amount of work extractable using global operations and that which are obtainable under local operations and classical communication [18]:

$$\Delta \equiv W_t - W_l, \quad (37)$$

where W_t denotes the maximum work extractable via global operations on the full system, and W_l is the localize information—that is, the work obtainable using only LOCC. Analogous to quantum discord, the work deficit admits an information-theoretic interpretation as the difference between the total correlation and its purely classical part.

Recently, Streltsov et al. [54,55] defined an asymmetric version known as the one-way information deficit using relative entropy. This measure has highlighted the role of quantum deficit as a genuine resource for entanglement distribution. When von Neumann measurements are performed on only one quantum subsystem, the one-way deficit is given by [56]

$$\Delta^{\rightarrow}(\rho^{ab}) = \min_{\{\Pi_k\}} S\left(\sum_k \Pi_k \rho^{ab} \Pi_k\right) - S(\rho^{ab}). \quad (38)$$

Although both the one-way deficit and quantum discord represent non-classical correlations, they are distinct quantities: they differ in their physical meaning, the class of allowed operations, and the nature of the required optimization. Since analytical expressions for quantum discord are available for certain structured two-qubit states—in particular X-shaped density matrices—it is natural to ask whether similar closed-form results can be obtained for the one-way deficit in the same state family. Here, we use the analytical

approach [57] that allows us to compute the one-way deficit exactly for the electron–proton state in the Hydrogen atom.

6. Numerical Results and Discussions

The parameters b_1, b_2, b_3 that define the initial Bell-diagonal X-state (Equation (17)) are restricted to the interval $[-1, 1]$ by positivity of the density operator. We adopt the representative values $b_1 = 1$, $b_2 = -0.8$, $b_3 = 0.8$, which satisfy the PPT separability criterion and therefore correspond to an initially separable state possessing only classical correlations. This choice is made deliberately so that any subsequent appearance of quantum dissonance or one-way deficit can be unambiguously attributed to the combined action of the hyperfine spin–spin interaction and the applied decoherence channels. The decoherence rate κ (reported in units of the hyperfine coupling α) is chosen in the range $\kappa = 0.02\alpha$ and 0.08α to illustrate the physically relevant competition between coherent spin dynamics and environmental noise. These dimensionless values lie well within the regime accessed in current experiments on hydrogen atoms, where coherence times are long compared with the hyperfine period.

In this section, we examine the temporal evolution of quantum dissonance and one-way quantum deficit. Utilizing the Lindblad formalism, we model two distinct decoherence scenarios: pure dephasing, which suppresses quantum coherences while preserving energy populations, and dissipative processes, which induce energy exchange with the environment. Through this comparative approach, we analyze how quantum dissonance and one-way quantum deficit deteriorate under contrasting noise mechanisms.

Figure 3 shows the time evolution of the quantum dissonance for the bipartite electron–proton density matrix in atomic hydrogen, subject to Markovian dephasing decoherence. The initial state is constructed on the hyperfine (Bell) basis with coefficients $b_1 = 1$, $b_2 = -0.8$, $b_3 = 0.8$. Two dephasing rates are considered: $\kappa = 0.02\alpha$ (blue curve) and $\kappa = 0.08\alpha$ (red curve), where α is the magnetic spin–spin coupling constant of the hydrogen ground-state hyperfine structure. The plot shows quantum dissonance $D(\rho)$ as a function of the dimensionless time variable t (scaled so that the natural frequency is set by α, i.e., physical time$\sim t/\alpha$). For both rates, dissonance emerges from an initially low value—consistent with the separable character of the prepared state—and exhibits a pronounced rise followed by a monotonic decay. The slower dephasing rate ($\kappa = 0.02\alpha$) allows significantly higher peak dissonance and sustained decay over longer times, reflecting weaker destruction of off-diagonal coherence terms that generate non-classical correlations. In contrast, the higher rate ($\kappa = 0.08\alpha$) rapidly suppresses the buildup and induces faster damping. This behavior underscores the robustness of dephasing-induced dissonance in the weak-coupling regime. Overall, the maxima in both curves mark the crossover from correlation-dominated dynamics to decoherence-dominated dynamics. An increase in the dephasing rate shifts this crossover to earlier times and reduces the maximum attainable quantum dissonance. Therefore, both the position and height of the critical points provide a clear quantitative characterization of how environmental noise constrains the generation and persistence of non-classical correlations in the electron–proton system.

Figure 4 presents the time evolution of the quantum dissonance for the same initial Bell-state–coefficient–parameterized electron–proton state, now subjected to Markovian dissipative decoherence. In contrast to the pure dephasing case, the dynamical behavior is qualitatively different. The dissonance again emerges from an initially nearly separable state, but it attains substantially lower peak values for the weaker dissipation rate compared to the stronger one and exhibits a monotonic increase followed by a steady saturation regime, without pronounced temporal modulations. The dissipative channel induces irreversible population transfer toward the ground hyperfine state, thereby more ef-

ficiently erasing both diagonal and off-diagonal contributions responsible for non-classical correlations. Consequently, even the weak dissipation rate suppresses dissonance much more effectively than equivalent-strength dephasing (as shown in Figure 3), highlighting the greater destructive impact of energy relaxation on quantum dissonance compared to pure phase noise. In both figures, the choice of Bell coefficients ensures that the initial state lies in the separable regime, allowing pure observation of dissonance emergence driven by tailored decoherence channels—a phenomenon with potential implications for engineering non-classical resources in spin-based atomic systems.

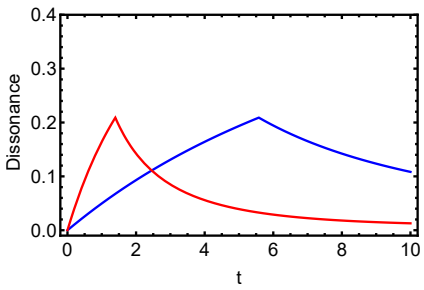


Figure 3. Time evolution of the quantum dissonance of the electron–proton density matrix for the dephasing case. The results correspond to initial conditions $b_1 = 1$, $b_2 = -0.8$, $b_3 = 0.8$ with dephasing rates $\kappa = 0.02\alpha$ (blue) and $\kappa = 0.08\alpha$ (red). Time t is given in units of $1/\alpha$. The non-monotonic behavior, including the peak, originates from a change in the ordering of the dominant eigenvalues entering the optimization procedure defining quantum dissonance, leading to a crossover between different spectral contributions under decoherence.

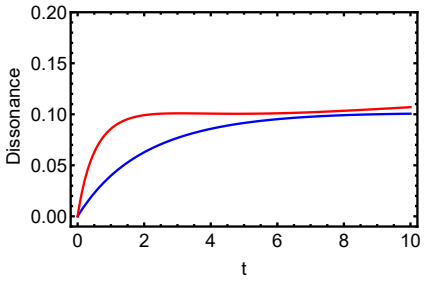


Figure 4. Time evolution of the quantum dissonance of the electron–proton density matrix for the dissipative case. The results correspond to initial conditions $b_1 = 1$, $b_2 = -0.8$, $b_3 = 0.8$ with dissipative rates $\kappa = 0.02\alpha$ (blue) and $\kappa = 0.08\alpha$ (red). Time t is given in units of $1/\alpha$. In this case, the dynamics exhibit a smooth decay without peak-like features, as the dominant eigenvalue structure remains unchanged and no spectral reordering occurs during the evolution.

Figure 5 depicts the temporal evolution of the one-way quantum information deficit (OWQID) in the electron–proton density matrix of a hydrogen atom, evaluated from Bell-state coefficients under dephasing decoherence. The OWQID is plotted as a function of dimensionless time t, for dephasing rates $\kappa = 0.02\alpha$ (blue curve) and $\kappa = 0.08\alpha$ (red curve), with initial conditions $b_1 = 1$, $b_2 = -0.8$, $b_3 = 0.8$. In the context of quantum theory, OWQID quantifies asymmetric non-classical correlations, defined as the minimum increase in entropy after a von Neumann measurement on one subsystem, reflecting the quantum advantage in information extraction beyond classical limits. Under dephasing, modeled by the Lindblad equation with phase-damping operators, the OWQID exhibits a monotonic decay from its initial value toward zero, indicative of the exponential suppression of coherences in the density matrix. The slower decay for the weaker dephasing rate demonstrates enhanced robustness against weak noise, while the stronger rate accelerates classicalization, approaching zero earlier. This behavior arises from the damping of off-diagonal elements at a rate proportional to κ, without population transfer. Consequently, OWQID's persistence

relative to entanglement measures underscores its utility in separable states, potentially enabling quantum-enhanced protocols in atomic hydrogen systems under noisy conditions.

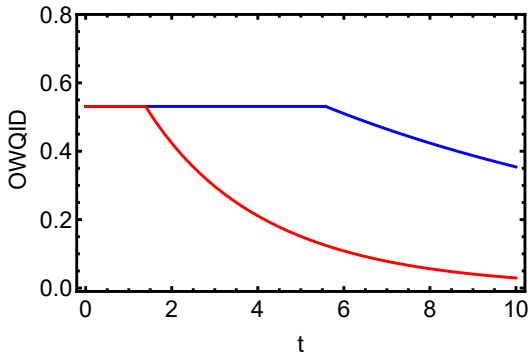


Figure 5. Time evolution of the one-way quantum information deficit (OWQID) of the electron–proton density matrix for the dephasing case. The results correspond to initial conditions $b_1 = 1$, $b_2 = -0.8$, $b_3 = 0.8$ with dephasing rates $\kappa = 0.02\alpha$ (blue) and $\kappa = 0.08\alpha$ (red). Time t is given in units of $1/\alpha$. An initial plateau is observed, where the OWQID remains constant, followed by a decay beyond a characteristic time. This transition is associated with a change in the dominant eigenvalue contributions entering the optimization procedure, reflecting a crossover from coherence-dominated to decoherence-dominated dynamics.

Figure 6 shows the time evolution of the one-way quantum information deficit in the electron–proton density matrix of a hydrogen atom, based on Bell-state coefficients under dissipative decoherence. The OWQID is plotted versus dimensionless time t, for dissipative rates $\kappa = 0.02\alpha$ and $\kappa = 0.08\alpha$, using the same initial conditions. Dissipative decoherence, governed by Lindblad operators inducing spin-flip transitions, models energy relaxation to the environment, affecting both coherences and populations in the hyperfine manifold. The OWQID decays gradually from its initial value to near zero, with the lower rate sustaining a small but notable value at $t = 10$, and the higher rate achieving classicality earlier. In comparison to dephasing (Figure 5), dissipation results in a lower initial OWQID and a more rapid decline for equivalent κ, attributable to the joint effects of coherence damping and population transfer toward the ground hyperfine state. This emphasizes the more pronounced influence of dissipation on quantum correlations in hydrogen atoms. The findings indicate that strategies to mitigate dissipative channels could help sustain OWQID for use in quantum technologies.

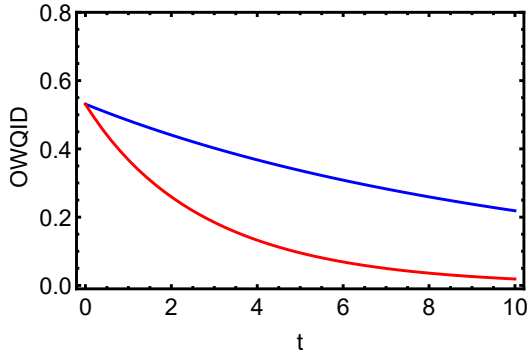


Figure 6. Time evolution of the one-way quantum information deficit (OWQID) of the electron–proton density matrix for the dissipative case. The results correspond to initial conditions $b_1 = 1$, $b_2 = -0.8$, $b_3 = 0.8$ with dissipative rates $\kappa = 0.02\alpha$ (blue) and $\kappa = 0.08\alpha$ (red). Time t is given in units of $1/\alpha$. In contrast to the dephasing case, the OWQID exhibits a monotonic decay, reflecting the combined effects of coherence loss and population relaxation, without the appearance of a plateau or crossover behavior.

The results presented in this work describe the dynamical behavior of quantum correlations in a two-qubit system comprising the electron and proton spin degrees of freedom of a hydrogen atom, under the influence of phase and amplitude damping channels. From a physical perspective, the system is governed by the competition between coherent hyperfine spin interactions and irreversible environmental decoherence.

The hyperfine interaction induces coherent exchange of spin excitations between the electron and proton, which is responsible for the nontrivial time dependence of the quantum correlations in the absence of noise. However, when the system is coupled to an external environment, decoherence mechanisms progressively suppress quantum coherences encoded in the off-diagonal elements of the density matrix. In the case of phase damping, this suppression affects only phase coherence. In contrast, amplitude damping additionally induces energy relaxation and population redistribution, leading to a generally faster degradation of quantum correlations.

At the level of the density matrix spectrum, the dynamics can be explicitly characterized in the Bell basis as follows. For the phase-damping (dephasing) channel, the eigenvalues are given by Equation (31), where the populations remain constant in time while only coherence-related contributions decay exponentially.

In contrast, for the amplitude-damping (dissipative) channel, the eigenvalues take the form Equation (32), where both coherence and population-related contributions decay due to the combined effects of dephasing and energy relaxation.

The time evolution of quantum dissonance and one-way quantum deficit can therefore be understood as a direct consequence of the above spectral dynamics. The decay of off-diagonal contributions encoded in the eigenvalue structure leads to the gradual suppression of quantum correlations, while residual diagonal contributions determine the long-time behavior.

The sharp changes observed in the temporal evolution of the quantum correlation measures, which may resemble "phase-transition-like" features in Figures 3 and 5, should not be interpreted as genuine phase transitions. Instead, they correspond to dynamical crossover regimes where the dominant physical mechanism changes from coherent hyperfine-driven evolution at short times to environment-induced decoherence at longer times.

An additional point clarifying the phase-transition-like behavior observed in Figures 3 and 5 is related to the ordering of the eigenvalues entering the definition of quantum measure. For evolution times shorter than the transition time, the two largest eigenvalues are λ_1 and λ_2, which determine the dominant contributions to the entropy-based quantities. However, beyond the transition time, a change in the spectral ordering occurs, such that λ_1 and λ_3 become the two largest eigenvalues, with λ_3 exceeding λ_2 (Figure 1).

This behavior does not appear in the dissipative case, where λ_1 and λ_2 remain the two largest eigenvalues throughout the entire time evolution, and no eigenvalue crossing or spectral reordering occurs (Figure 2). This crossover in the eigenvalue hierarchy induces a non-analytic change in the structure of the optimization underlying quantum dissonance, which manifests as the observed phase-transition-like feature in Figures 3 and 5. It should therefore be interpreted as a spectral reordering effect rather than a genuine thermodynamic phase transition. The saturation behavior observed in the long-time limit, particularly in Figure 4, can be understood in terms of the asymptotic steady-state solution of the Lindblad master equation. In this regime, the system approaches a stationary mixed state determined entirely by the dissipative channels, where quantum coherences vanish while classical mixtures persist. Consequently, the quantum correlation measures converge to constant asymptotic values.

Finally, the eigenvalue dynamics provide a complementary picture of the loss of purity and redistribution of quantum information under decoherence. The transition from time-dependent to effectively stationary eigenvalues reflects the approach to the steady-state manifold and fully explains the asymptotic behavior of all correlation measures considered in this work.

Overall, the observed dynamics can be physically interpreted as the decay of initially present quantum correlations due to the combined action of hyperfine interaction and environmental decoherence, with the long-time behavior governed by the Lindblad steady-state structure.

Finally, we briefly comment on the possible impact of non-Markovian effects on the present results. The Markovian approximation adopted in this work neglects memory effects arising from system–environment correlations. In more realistic scenarios, non-Markovian dynamics may induce information backflow from the environment to the system, leading to non-monotonic behavior and possible revivals of quantum correlations. In particular, as shown in Ref. [58], quantum correlations such as discord-like measures can exhibit enhanced robustness and even temporary amplification under non-Markovian conditions. A systematic extension of the present analysis to such regimes would therefore provide further insight into the persistence of non-classical correlations in open quantum systems.

From an experimental perspective, the hyperfine electron–proton spin system considered in this work can be realized or effectively simulated in several well-established quantum platforms. A prominent example is atomic hydrogen stabilized in solid molecular hydrogen matrices at cryogenic temperatures, where high-density ensembles of H defects can be created and investigated using electron spin resonance (ESR) and nuclear magnetic resonance (NMR) techniques [59,60]. These experiments demonstrate long spin coherence times and provide direct access to relaxation and decoherence mechanisms in the millikelvin regime.

In addition, spin-polarized atomic hydrogen gases confined in magnetic traps constitute another experimentally relevant platform, where hyperfine-state dynamics can be controlled and probed with high precision. In such systems, decoherence mainly originates from magnetic-field inhomogeneities, spin exchange, and spin–lattice relaxation processes, which can be effectively modeled through Markovian dephasing and amplitude-damping channels. Beyond atomic hydrogen, analogous hyperfine-like spin interactions are routinely engineered in several controllable quantum information platforms, including trapped-ion systems, nitrogen-vacancy (NV) centers in diamond, semiconductor donor-spin qubits, and NMR-based quantum simulators [61–64]. In these systems, coherent spin coupling and environmentally induced decoherence can be tuned experimentally, enabling direct investigations of the robustness and dynamics of quantum correlations in open two-qubit systems.

Consequently, the parameters entering our Lindblad description can be directly connected to experimentally measurable relaxation and decoherence rates in modern spin-based quantum platforms.

7. Conclusions

In conclusion, this study has analyzed the emergence and dynamical behavior of quantum correlations, specifically quantum dissonance and one-way quantum deficit, in a separable electron–proton spin system modeling the hyperfine structure of the hydrogen atom. Within a two-qubit framework, we have shown that non-classical correlations can arise from initially separable states due to the intrinsic spin–spin interaction. The analytical and numerical investigations of their time evolution under dephasing and dissipative

environments reveal a gradual decay of quantum correlations, whose behavior is governed by the competition between coherent hyperfine dynamics and environmental decoherence. In particular, both quantum dissonance and one-way quantum deficit exhibit a relatively slow degradation under noise, maintaining non-vanishing values over extended time scales depending on the strength of the dissipation. These results highlight the robustness of certain forms of quantum correlations in open quantum systems, even in the absence of entanglement. The observed dynamics underscore the role of system–environment interactions in shaping the persistence of quantum features in spin-based systems. Finally, the present analysis provides a useful framework for understanding correlation dynamics in effective two-qubit atomic models. Extensions of this work to non-Markovian environments or multi-spin systems may further clarify the interplay between coherence preservation and environmental memory effects in more complex quantum settings. Overall, these results contribute to a clearer understanding of how different types of quantum correlations evolve under decoherence in minimal spin systems. They also provide a useful benchmark for analyzing correlation robustness in generic two-qubit open quantum models.

Author Contributions: Writing—original draft, K.B. and S.B.; Writing—review and editing, K.B. and S.B. All authors have read and agreed to the published version of the manuscript.

Funding: This work was supported and funded by the Deanship of Scientific Research at Imam Mohammad Ibn Saud Islamic University (IMSIU) (grant number IMSIU-DDRSP2603).

Data Availability Statement: The original contributions presented in this study are included in the article. Further inquiries can be directed to the corresponding author.

Conflicts of Interest: The authors declare no conflicts of interest.

Appendix A. Separability of the State in Equtaion (35)

In this Appendix A, we show that the state defined in Equtaion (35),

$$\hat{\sigma} = \sum_{i=1}^{4} p_i |\Psi_i\rangle\langle\Psi_i|, \tag{A1}$$

is separable for the choice of probabilities specified in the main text.

Since $\hat{\sigma}$ is a Bell-diagonal state, its separability can be determined using the Peres–Horodecki (PPT) criterion [1,65,66], which is necessary and sufficient for two-qubit systems. A Bell-diagonal state is separable if and only if its largest eigenvalue satisfies

$$\max_i \, p_i \leq \frac{1}{2}. \tag{A2}$$

In our case, we have $p_1 = 1/2$, while the remaining probabilities are given by

$$p_i = \frac{\lambda_i}{2(1-\lambda_1)}, \quad i = 2, 3, 4, \tag{A3}$$

with $\sum_i p_i = 1$.

It follows immediately that $p_1 = 1/2$ is the largest eigenvalue, while for $i = 2, 3, 4$, one has $p_i \leq 1/2$ since $\lambda_i \leq 1 - \lambda_1$. Therefore,

$$\max_i p_i = \frac{1}{2}, \tag{A4}$$

which satisfies the separability condition.

Hence, the state $\hat{\sigma}$ is separable, lying on the boundary between separable and entangled Bell-diagonal states.

References

1. Modi, K.; Paterek, T.; Son, W.; Vedral, V.; Williamson, M. Classical and quantum correlations *Phys. Rev. Lett.* **2010**, *104*, 080501. [CrossRef]
2. Nielsen, M.A.; Chuang, I.L. Quantum Computation and Quantum Information; Cambridge University Press: Cambridge, UK, 2000.
3. Bennett, C.H.; Brassard, G.; Crépeau, C.; Jozsa, R.; Peres, A.; Wootters, W.K. Teleporting an Unknown Quantum State via Dual Classical and Einstein-Podolsky-Rosen Channels. *Phys. Rev. Lett.* **1993**, *70*, 1895. [CrossRef]
4. Bennett, C.H.; Wiesner, S.J. Communication via one- and two-particle operators on Einstein-Podolsky-Rosen states. *Phys. Rev. Lett.* **1992**, *69*, 2881–2884. [CrossRef] [PubMed]
5. Ekert, A.K. Quantum cryptography based on Bell's theorem. *Phys. Rev. Lett.* **1991**, *67*, 661–663. [CrossRef] [PubMed]
6. Pati, A.K. Minimum classical bit for remote preparation and measurement of a quantum state. *Phys. Rev. A* **2000**, *63*, 014302. [CrossRef]
7. Bennett, C.H.; DiVincenzo, D.P.; Fuchs, C.A.; Mor, T.; Rains, E.; Shor, P.W.; Smolin, J.A.; Wootters, W.K. Remote state preparation. *Phys. Rev. Lett.* **2001**, *87*, 077902. [CrossRef]
8. Henderson, L.; Vedral, V. Classical, quantum and total correlations. *J. Phys. A* **2001**, *34*, 6899–6905. [CrossRef]
9. Ollivier, H.; Zurek, W.H. Quantum discord: A measure of the quantumness of correlations. *Phys. Rev. Lett.* **2002**, *88*, 017901. [CrossRef]
10. Giorgi, G.L.; Galve, F.; Zambrini, R. Genuine quantum and classical correlations in multipartite systems. *Phys. Rev. Lett.* **2011**, *107*, 190501. [CrossRef] [PubMed]
11. Streltsov, A.; Kampermann, H.; Bruß, D. Are general quantum correlations monogamous? *Phys. Rev. Lett.* **2012**, *109*, 050503. [CrossRef]
12. Modi, K.; Brodutch, A.; Cable, H.; Paterek, T.; Vedral, V. The classical-quantum boundary for correlations. *Rev. Mod. Phys.* **2012**, *84*, 1655–1707. [CrossRef]
13. Ali, M.; Rau, A.R.P.; Alber, G. Quantum discord for two-qubit X states *Phys. Rev. A* **2010**, *81*, 042105. [CrossRef]
14. Li, B.; Wang, Z.X.; Fei, S.M. Quantum discord and geometry for a class of two-qubit states. *Phys. Rev. A* **2011**, *83*, 022321. [CrossRef]
15. Chen, Q.; Zhang, C.; Yu, S.; Yi, X.X.; Oh, C.H. Quantum discord of two-qubit X states. *Phys. Rev. A* **2011**, *84*, 042313. [CrossRef]
16. Shi, M.; Sun, C.P.; Jiang, F.; Yan, X.; Du, J. Optimal measurement for quantum discord of two-qubit states. *Phys. Rev. A* **2012**, *85*, 064104. [CrossRef]
17. Vinjanampathy, S.; Rau, A.R.P. Quantum discord for qubit systems: A geometrical perspective. *J. Phys. A Math. Theor.* **2012**, *45*, 095303. [CrossRef]
18. Oppenheim, J.; Horodecki, M.; Horodecki, P.; Horodecki, R. Thermodynamical approach to quantifying quantum correlations. *Phys. Rev. Lett.* **2002**, *89*, 180402. [CrossRef]
19. Horodecki, M.; Horodecki, P.; Horodecki, R.; Oppenheim, J. Local versus nonlocal information in quantum-information theory: formalism and applications. *Phys. Rev. Lett.* **2003**, *90*, 100402. [CrossRef]
20. Luo, S. Quantum discord for two-qubit systems. *Phys. Rev. A* **2008**, *77*, 042303. [CrossRef]
21. Dakić, B.; Vedral, V.; Brukner, Č. Necessary and sufficient condition for nonzero quantum discord. *Phys. Rev. Lett.* **2010**, *105*, 190502. [CrossRef]
22. Luo, S.; Fu, S. Geometric measure of quantum discord. *Phys. Rev. A* **2010**, *82*, 034302. [CrossRef]
23. Adesso, G.; Datta, A. Quantum versus classical correlations in Gaussian states. *Phys. Rev. Lett.* **2010**, *105*, 030501. [CrossRef]
24. Giorda, P.; Paris, M.G.A. Gaussian quantum discord. *Phys. Rev. Lett.* **2010**, *105*, 020503. [CrossRef]
25. Bohr, N. On the constitution of atoms and molecules. *Philos. Mag.* **1913**, *26*, 1–25. [CrossRef]
26. Bethe, H.A.; Salpeter, E.E. *Quantum Mechanics of One- and Two-Electron Atoms*; Springer: Berlin/Heidelberg, Germany, 1957.
27. Series, G.W. *The Spectrum of Atomic Hydrogen*; Oxford University Press: New York, NY, USA, 1957.
28. Landau, L.D.; Lifshitz, E.M. *Quantum Mechanics: Non-Relativistic Theory*, 3rd ed.; Elsevier: Amsterdam, The Netherlands, 1977.
29. Sheludiakov, S.; McColgan, P.T.; Lee, D.M.; Khmelenko, V.V.; Järvinen, J.; Ahokas, J.; Vasiliev, S.V. Formation of Nuclear-Polarized Phases of H Atoms Embedded in Solid H_2 Films. *Phys. Rev. Lett.* **2019**, *122*, 225301. [CrossRef]
30. Ahokas, J.; Järvinen, J.; Khmelenko, V.V.; Lee, D.M.; Vasiliev, S. Exotic Behavior of Hydrogen Atoms in Solid H_2 at Temperatures below 1 K. *Phys. Rev. Lett.* **2006**, *97*, 095301. [CrossRef]

31. Ahokas, J.; Vainio, O.; Novotny, S.; Järvinen, J.; Khmelenko, V.V.; Lee, D.M.; Vasiliev, S. Magnetic resonance study of H atoms in thin films of H_2 at temperatures below 1 K. *Phys. Rev. B* **2010**, *81*, 104516. [CrossRef]
32. Bigelow, N.P.; Freed, J.H.; Lee, D.M. Nuclear-spin waves in polarized atomic hydrogen gas: Temperature and density dependence in the hydrodynamic and Knudsen regimes. *Phys. Rev. Lett.* **1989**, *63*, 1609–1612. [CrossRef] [PubMed]
33. Johnson, A.C.; Petta, J.R.; Marcus, C.M.; Hanson, M.P.; Gossard, A.C. Triplet–singlet spin relaxation via nuclei in a double quantum dot. *Nature* **2005**, *435*, 925–928. [CrossRef]
34. Petta, J.R.; Johnson, A.C.; Taylor, J.M.; Laird, E.A.; Yacoby, A.; Lukin, M.D.; Marcus, C.M.; Hanson, M.P.; Gossard, A.C. Coherent manipulation of coupled electron spins in semiconductor quantum dots. *Science* **2005**, *309*, 2180–2184. [CrossRef]
35. Taylor, J.M.; Engel, H.A.; Dür, W.; Yacoby, A.; Marcus, C.M.; Zoller, P.; Lukin, M.D. Fault-tolerant architecture for quantum computation using electrically controlled semiconductor spins. *Nat. Phys.* **2005**, *1*, 177–183. [CrossRef]
36. Ladd, T.D.; Jelezko, F.; Laflamme, R.; Nakamura, Y.; Monroe, C.; O'Brien, J.L. Quantum computers. *Nature* **2010**, *464*, 45–53. [CrossRef]
37. Bennett, C.H.; DiVincenzo, D.P. Quantum information and computation. *Nature* **2000**, *404*, 247–255. [CrossRef] [PubMed]
38. Childress, L.; Dutt, M.V.G.; Taylor, J.M.; Zibrov, A.S.; Jelezko, F.; Wrachtrup, J.; Hemmer, P.R.; Lukin, M.D. Coherent dynamics of coupled electron and nuclear spin qubits in diamond. *Science* **2006**, *314*, 281–285. [CrossRef] [PubMed]
39. Dutt, M.V.G.; Childress, L.; Jiang, L.; Togan, E.; Maze, J.; Jelezko, F.; Zibrov, A.S.; Hemmer, P.R.; Lukin, M.D. Quantum register based on individual electronic and nuclear spin qubits in diamond. *Science* **2007**, *316*, 1312–1316. [CrossRef]
40. Neumann, P.; Mizuochi, N.; Rempp, F.; Hemmer, P.; Watanabe, H.; Yamasaki, S.; Jacques, V.; Gaebel, T.; Jelezko, F.; Wrachtrup, J. Multipartite entanglement among single spins in diamond. *Science* **2008**, *320*, 1326–1329. [CrossRef]
41. Fuchs, G.D.; Dobrovitski, V.V.; Toyli, D.M.; Heremans, F.J.; Awschalom, D.D. Gigahertz dynamics of a strongly driven single quantum spin. *Science* **2009**, *326*, 1520–1522. [CrossRef]
42. von Neumann, J. *Mathematical Foundations of Quantum Mechanics*; Princeton University Press: Princeton, NJ, USA, 1955.
43. Benatti, F.; Floreanini, R. *Open Quantum Systems*; Springer: Berlin/Heidelberg, Germany, 2003.
44. Preskill, J. *Lecture Notes for Physics 229: Quantum Information and Computation*; California Institute of Technology: Pasadena, CA, USA, 1998
45. Demtröder, W. *Atoms, Molecules and Photons*; Springer Berlin/Heidelberg, Germany, 2010; Volume 3.
46. Pethick, C.J.; Smith, H. *Bose–Einstein Condensation in Dilute Gases*; Cambridge University Press: Cambridge, UK, 2008.
47. Maleki, Y.; Sheludiakov, S.; Khmelenko, V.V.; Scully, M.O.; Lee, D.M.; Zheltikov, A.M. Natural and magnetically induced entanglement of hyperfine-structure states in atomic hydrogen. *Phys. Rev. A* **2021**, *103*, 052804. [CrossRef]
48. Nathan, F.; Rudner, M.S. Universal Lindblad equation for open quantum systems. *Phys. Rev. B* **2020**, *102*, 115109. [CrossRef]
49. Manzano, D. A short introduction to the Lindblad master equation. *AIP Adv.* **2020**, *10*, 025106. [CrossRef]
50. Budini, A.A. Lindblad rate equations. *Phys. Rev. A* **2006**, *74*, 053815. [CrossRef]
51. Bouwmeester, D.; Pan, J.-W.; Mattle, K.; Eibl, M.; Weinfurter, H.; Zeilinger, A. Experimental quantum teleportation. *Nature* **1997**, *390*, 575–579. [CrossRef]
52. Furusawa, A.; Sørensen, J.L.; Braunstein, S.L.; Fuchs, C.A.; Kimble, H.J.; Polzik, E.S. Unconditional quantum teleportation. *Science* **1998**, *282*, 706–709. [CrossRef] [PubMed]
53. Maleki, Y.; Zheltikov, A.M. Optical control of spin coherence in atomic hydrogen systems. *Opt. Express* **2019**, *27*, 8291–8307. [CrossRef]
54. Streltsov, A.; Kampermann, H.; Bruß, D. Quantum cost for sending entanglement. *Phys. Rev. Lett.* **2012**, *108*, 250501. [CrossRef]
55. Chuan, T.K.; Maillard, J.; Modi, K.; Paterek, T.; Paternostro, M.; Piani, M. Quantum discord bounds the amount of distributed entanglement. *Phys. Rev. Lett.* **2012**, *109*, 070501. [CrossRef] [PubMed]
56. Streltsov, A.; Kampermann, H.; Bruß, D. Linking quantum discord to entanglement in a measurement. *Phys. Rev. Lett.* **2011**, *106*, 160401. [CrossRef]
57. Eftekhari, H.; Faizi, E. The one-way information deficit for a class of two-qubit states. *Int. J. Quantum Inf.* **2015**, *13*, 1550012. [CrossRef]
58. Shen, H.Z.; Wang, Q.; Wang, J.; Yi, X.X. Nonreciprocal unconventional photon blockade in a driven dissipative cavity with parametric amplification. *Phys. Rev. A* **2020**, *101*, 013826. [CrossRef]
59. Wetzel, C.K.; Lee, D.M.; Sheludiakov, S.; Ahokas, J.; Vasiliev, S.; Khmelenko, V.V. Studies of hydrogen atom recombination in solid hydrogen deuteride. *J. Low Temp. Phys.* **2025**, *220*, 104–114. [CrossRef]
60. Sheludiakov, S.; Ahokas, J.; Järvinen, J.; Vasiliev, S.; Wetzel, C.K.; Lee, D.M.; Khmelenko, V.V. Broad central line observed in electron spin resonance experiments on hydrogen atom isotopes in solid molecular films of hydrogen isotopes. *Phys. Rev. B* **2024**, *110*, 224106. [CrossRef]
61. Blatt, R.; Roos, C.F. Quantum simulations with trapped ions. *Nat. Phys.* **2012**, *8*, 277–284. [CrossRef]
62. Doherty, M.W.; Manson, N.B.; Delaney, P.; Jelezko, F.; Wrachtrup, J.; Hollenberg, L.C. The nitrogen-vacancy colour centre in diamond. *Phys. Rep.* **2013**, *528*, 1–45. [CrossRef]

63. Kane, B.E. A silicon-based nuclear spin quantum computer. *Nature* **1998**, *393*, 133–137. [CrossRef]
64. Cory, D.G.; Fahmy, A.F.; Havel, T.F. Ensemble quantum computing by NMR spectroscopy. *Proc. Natl. Acad. Sci. USA* **1997**, *94*, 1634–1639. [CrossRef]
65. Peres A. Separability Criterion for Density Matrices. *Phys. Rev. Lett.* **1996**, *77*, 1413–1415. [CrossRef]
66. Horodecki, M.; Horodecki, P.; Horodecki, R. Separability of Mixed States: Necessary and Sufficient Conditions. *Phys. Lett. A* **1996**, *223*, 1–8. [CrossRef]

Disclaimer/Publisher's Note: The statements, opinions and data contained in all publications are solely those of the individual author(s) and contributor(s) and not of MDPI and/or the editor(s). MDPI and/or the editor(s) disclaim responsibility for any injury to people or property resulting from any ideas, methods, instructions or products referred to in the content.